Electrochemistry Communications 161 (2024) 107683

Contents lists available at ScienceDirect

Electrochemistry Communications

journal homepage: www.elsevier.com/locate/elecom

Nanostructured and porous antimony-doped tin oxide as electrode material for the heat-to-electricity energy conversion in thermo-electrochemical cells

Sergio Castro-Ruiz, Jorge García-Cañadas *

Department of Industrial Systems Engineering and Design, Universitat Jaume I, Av. Vicent Sos Baynat s/n, 12006 Castelló de la Plana, Spain

ARTICLE INFO

Keywords:
Thermocell
Thermogalvanic cell
Metal oxide
ATO
Porous electrode

ABSTRACT

Thermo-electrochemical cells (or thermogalvanic cells or thermocells, TECs) have gained attention as devices able to convert low temperature heat into electricity. Within TECs, Pt is one of the most employed electrodes, since it exhibits a fast transfer of electrons with the redox couple in the electrolyte. However, its high price represents a serious drawback. Here, we analyze the use of nanostructured and porous antimony-doped tin oxide ($Sb:SnO_2$) as electrode material. Electrodes of different thickness (320, 550 and 1550 nm) were fabricated by spin coating to study the effect of the electrode area in contact with the electrolyte. $F:SnO_2$ (FTO) glass was used as a substrate and the typical 0.4 M potassium ferro/ferricyanide aqueous solution served as electrolyte. An impedance spectroscopy analysis under operating conditions (10 K temperature difference) showed that the $Sb:SnO_2$ electrodes exhibit the same excellent kinetics as Pt for all the different thickness. On the other hand, the power output density was thickness independent, since the temperature coefficients and the series and mass-transport resistances were similar, leading to no performance improvements when the electrode area in contact with the electrolyte was significantly increased. Finally, the Carnot-related efficiencies estimated for the $Sb:SnO_2$ cells were in the same order of magnitude as for Pt electrodes. These results open the possibility to use $Sb:SnO_2$ as a suitable electrode in TECs at low cost.

1. Introduction

Our planet is currently facing a very critical situation related to the high energy demand imposed by our society. This demand is still mostly covered by the use of fossil fuels, which produce large amounts of greenhouse gases that are causing the global warming. Under this scenario, it is imperative to develop more sustainable and environmentally friendly energy routes [1]. More than 60 % of the total energy used is lost as waste heat, being more than 80 % at low temperature (<100 °C) [2]. Therefore, it would be highly convenient to use this vast amount of energy cleanly, sustainably and cheaply in order to obtain useful energy (e.g. electricity) [3,4].

Thermo-electrochemical cells (or thermocells, or thermogalvanic cells, TECs) have gained attention in the last decade due to their capability to produce electricity by using low-temperature heat [5,6]. Liquid TECs are formed by two electrodes (usually Pt) in contact with a solution that contains a redox couple (electrolyte). The benchmark TEC consists of two Pt electrodes in contact with an aqueous solution of 0.4 M potassium ferro/ferricyanide [7]. When a temperature difference ΔT is present, these devices generate an open-circuit voltage V_{oc} due to the temperature dependency of the redox couple potential. One of the main advantages of TECs is that their temperature coefficient α (also called Seebeck coefficient) is in the order of mV/K, which is one/two orders of magnitude higher than in solid-state thermoelectric materials. However, their efficiency η and Carnot-related efficiency [$\eta_r = \eta/(\Delta T/T_H)$, being T_H the hot side temperature] values are still low (below 0.1 % and 1.0 %, respectively) in most of the cases, mainly due to their high electric resistance [8]. In addition, the commonly used electrode, Pt, is very expensive, which is another serious drawback for their widespread application.

Suitable electrodes for TECs should have high electrical conductivity to effectively transport the electrons to/from the external circuit and small charge-transfer resistance (fast exchange of electrons between the redox species and the electrodes) at low cost. Several alternative electrodes to Pt have been reported, many of them exhibiting porosity to achieve a large surface area to minimize the charge-transfer resistance.

* Corresponding author.
E-mail address: garciaj@uji.es (J. García-Cañadas).

https://doi.org/10.1016/j.elecom.2024.107683
Received 17 January 2024; Received in revised form 20 February 2024; Accepted 24 February 2024
Available online 25 February 2024

Some examples are carbon-based electrodes [9] such as single- and multi-walled carbon nanotubes [10,11] or aerogel-printed carbon nanotubes [12]. In addition, increasing the electrolyte concentration has been reported to be an effective method to obtain large power outputs in TECs [13]. In this sense, concentrations up to 2.4 m were obtained for the ferro/ferricyanide electrolyte producing the so-called water-in-salt electrolyte. Furthermore, a 0.9 M concentration was achieved by replacing K^+ by NH_4^+ cations in the same electrolyte increasing the power output [9].

Here, we explore the use of nanostructured and porous antimony-doped tin oxide Sb:SnO_2 (ATO) as electrode in TECs. Porous metal oxides, like ATO, are used as electrodes in different energy-related systems, such as batteries [14], solar cells [15] and supercapacitors [16], where they show high chemical stability and large surface area. Nevertheless, these metal oxides have been hardly employed in TECs, although they have been reported to display good electrochemical behaviour [17]. To our knowledge, there are only two cases in the literature. On one hand, it was reported the use of nanostructured Ni/NiO micro-sphered electrodes in a TEC that achieved a power density value of 1.72 W/m^2 [18]. On the other hand, a record of $\eta_r = 14.8$ % was recently achieved using asymmetric CoO electrodes in contact with a guanidium-boosted Fe$(CN)_6^{-3/-4}$ electrolyte [19]. In this article, we have prepared ATO films deposited on fluorine-doped tin oxide (FTO) coated glass substrates which also act as current collectors. The standard 0.4 M potassium ferro/ferricyanide aqueous electrolyte was used as electrolyte. We studied the effect of the ATO thickness and compared the performance with the standard Pt electrodes, obtaining similar behaviors.

2. Experimental part

Nanostructured and porous Sb:SnO_2 films were fabricated following a previously described procedure [20] using FTO-coated glasses of 25 mm x 25 mm size and 2.2 mm thickness as substrates (Sigma Aldrich, 735167-EA). These substrates were cleaned before the ATO film deposition by means of three sonication steps of 15 min in different media. In the first step, sonication was performed using a soap (Labkem, SOAP-0685 K0)/water solution (1:10 v/v). Then, distilled water to remove soap excess was used as second step. Finally, isopropanol (Labkem, PROL-P0P-5 K0) media was employed for sonication. After this, substrates were dried under compressed air flow and treated in a UV-ozone cleaner (Ossila, L2002A2-UK) for 20 min. Subsequently, an Sb:SnO_2 colloidal aqueous dispersion (Keeling & Walker, A20W) was deposited by spin coating (Laurell, WS-650MZ-23NPPB) at 2500 rpm for 15 s, covering a centered area of the substrate of 15 mm × 15 mm. Several layers (2, 5 and 10) were deposited. After each deposition, a drying process was carried out on a hot plate at 100 °C for 10 min. Finally, the films were annealed at 550 °C for 45 min in a furnace (Nabertherm, 400–1) with a 3 °C/min heating rate. Scanning electron microscopy (SEM) images of the films were obtained using a JEOL 7001F instrument (Oxford Instruments).

Five different symmetrical TECs were prepared. Three of them using the FTO/ATO electrodes with the different number of ATO layers (2, 5 and 10). Another cell was fabricated using Pt electrodes, which were prepared by depositing Pt by sputtering (Quorum, Q300T D Plus) on FTO glass during 6 min. The last TEC employed only FTO glass as electrodes. All these electrodes can be seen in Fig. 1a. To improve the electrical contact, certain area of the electrodes was painted with Ag paint (RS, 186–3600), as also shown in Fig. 1a. A solution of 0.4 M potassium ferrocyanide (Sigma Aldrich, P3289-100G) and 0.4 M potassium ferricyanide (Fluka, BCBT1564) in milli-Q water was employed as electrolyte in all the cells. All the chemicals were used as received.

A custom setup was built up to characterize the fabricated TECs (see Fig. 1b, c). In order to establish a temperature difference in the setup, two copper blocks were employed. One of them, with 30 mm × 30 mm × 10 mm dimensions and 2 cartridge heaters inserted (Watlow, C1A-9604), acted as the heat source. The heaters were powered using a Keithley 2601 source meter. A second larger copper block (40 mm × 40 mm × 10 mm, Tangxi X00170O3IZ) with a water circulation channel was used as the heat sink. A water circulator (PolySicence, SD07R-20-A12E) was employed to circulate the water at a certain temperature along the Cu block.

The electrodes for each cell were centered on top of the copper blocks. Thermal grease (RS, 1938247) was used at all the glass/Cu interfaces to improve the thermal contacts. The electrodes were separated by a polytetrafluoroethylene (PTFE) cell which contained the electrolyte in a cylindrical channel of 10 mm length and 4 mm diameter. The channel connected to two top holes for the injection of the electrolyte. These holes were covered with tape after inserting the electrolyte to

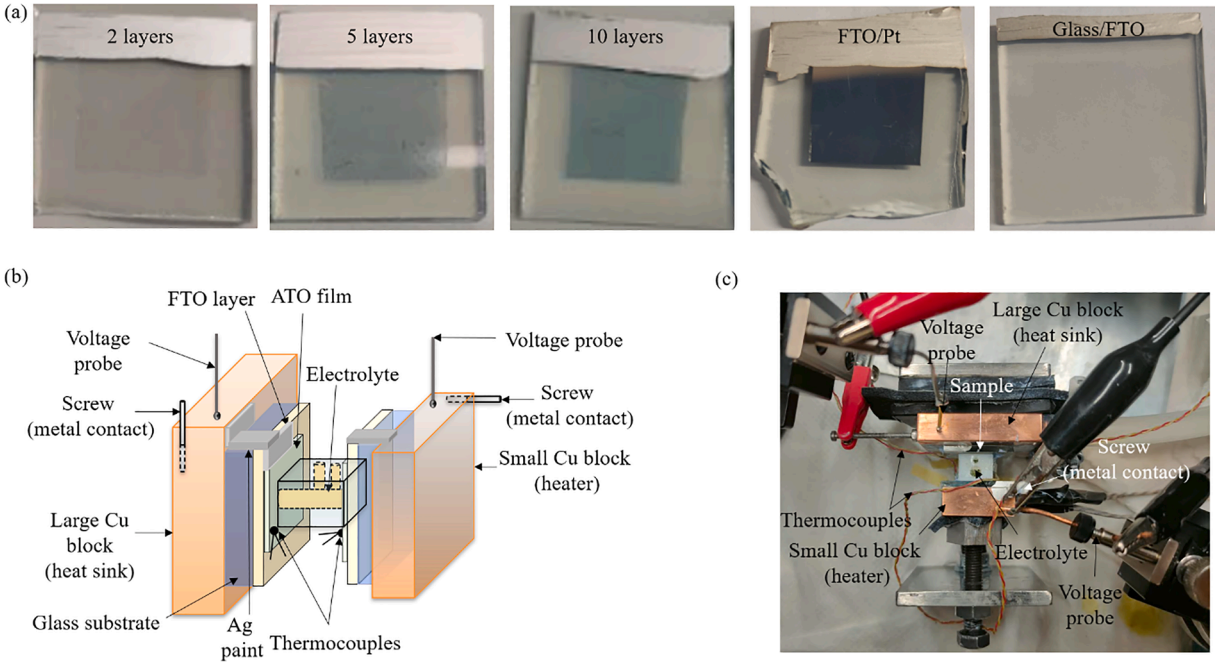

Fig. 1. (a) Different electrodes fabricated. (b) Scheme and (c) picture of the setup employed.

avoid evaporation (see Fig. 1b, c).

To avoid electrolyte leakage, two O-rings were located at the sides of the PTFE cell and were pressed against the electrodes by a system formed by stainless steel plates and screws. The area delimited by the O-rings, which determines the geometrical area A of the electrodes in contact with the electrolyte, was 0.5 cm^2. Two stainless steel screws inserted in the Cu blocks were used as electrical contacts for the current flow. In addition, two spring probes were contacted on top of the Cu blocks and were employed to sense the voltage (see Fig. 1b, c). The Cu blocks were electrically connected to the electrodes by extending the Ag paint (see Fig. 1b, c).

The temperature coefficient α, which indicates the variation of the open-circuit potential V_{oc} with the temperature difference, was obtained from the slope of a V_{oc} vs ΔT plot. The V_{oc} was measured with a Keithley 2100 nanovoltmeter, and the temperature difference was increased in steps of ≈2.5 K, from 0 up to ≈10 K, keeping the cold side temperature fixed at 25.0 °C. Two K-type thermocouples (RS, 8140134) and a dual thermometer (RS, 123–2214) were used to monitor the hot (T_H) and cold-side (T_C) temperatures. The thermocouples were placed on top of the electrodes, close to the PTFE cell, with a bit of thermal grease at their tips for thermalisation (see Fig. 1b, c).

To evaluate the performance of the TECs, impedance spectroscopy (IS) was used. IS measurements were carried out at the V_{oc} value when the cells were under a $\Delta T = 10$ K ($T_C = 25.0$ °C) using an amplitude of 15 mV in a frequency range from 1 MHz to 1 mHz. A Metrohm-Autolab PGSTAT204 potentiostat equipped with a FRA32M frequency response analyzer controlled by Nova 1.11 software was used. ZView 3.5 h was employed to fit the experimental impedance results to different equivalent circuits.

3. Results and Discusion

Fig. 2 shows the SEM images of the different Sb:SnO_2 films prepared. It can be seen that the films are formed by interconnected nanoparticles of sizes below 10 nm. Also, pores are present with sizes not larger than c. a. 30 nm (see inset of Fig. 2a). The thickness of the films can be estimated from the cross-sectional views (see Fig. 2b-d). For the films with 2, 5 and 10 layers, thickness values of 320, 550 and 1550 nm were found. It should be noted that the expected phase (cassiterite SnO_2) was previously identified by XRD experiments in our previous article [20]. Also, it can be seen in that reference that no changes in the XRD patterns were observed after the annealing process. Similarly, an EDX analysis from the same article showed no changes in the chemical composition of the film after the thermal treatment.

To evaluate the performance of the different TECs prepared, IS measurements at the open-circuit voltage (under $\Delta T = 10$ K) were performed. Fig. 3 shows the results obtained for each cell with their corresponding fittings, performed using the equivalent circuits in the insets. The fitted parameters with their corresponding errors are shown in Table 1. For the TECs with the ATO and Pt electrodes, an equivalent circuit formed by a series resistance R_s (accounting for the cables, contacts and electrolyte resistances) and the finite-length Warburg impedance with a transmissive boundary (short circuit terminus W_s), both connected in series, was used (see Fig. 3a). The impedance of the W_s element is defined as $Z_{Ws} = R_{mt}\,(j\omega d^2/D)^{-p}\,\tanh[(j\omega d^2/D)^p]$, being R_{mt} the mass-transport resistance, related to the diffusion of the redox species to/from the electrodes, $j=(-1)^{0.5}$, ω the angular frequency, d the diffusion length (distance between electrodes), D the diffusion coefficient of the redox species (assumed equal for both molecules) and p an exponent, which accounts for deviations from the ideal value ($p = 0.5$) [21,22].

For the TEC with only FTO electrodes, two additional elements were added to the equivalent circuit, a charge-transfer resistance R_{ct}, related to the kinetics of the transfer of electrons between the redox species and the electrodes, and a double-layer capacitor, accounting for the accumulation of charge at the electrode/electrolyte interface (see Fig. 3b). These two elements (R_{ct} and C_{dl}) produce the semicircle observed in Fig. 3b, which has also been observed before [23]. This semicircle is not

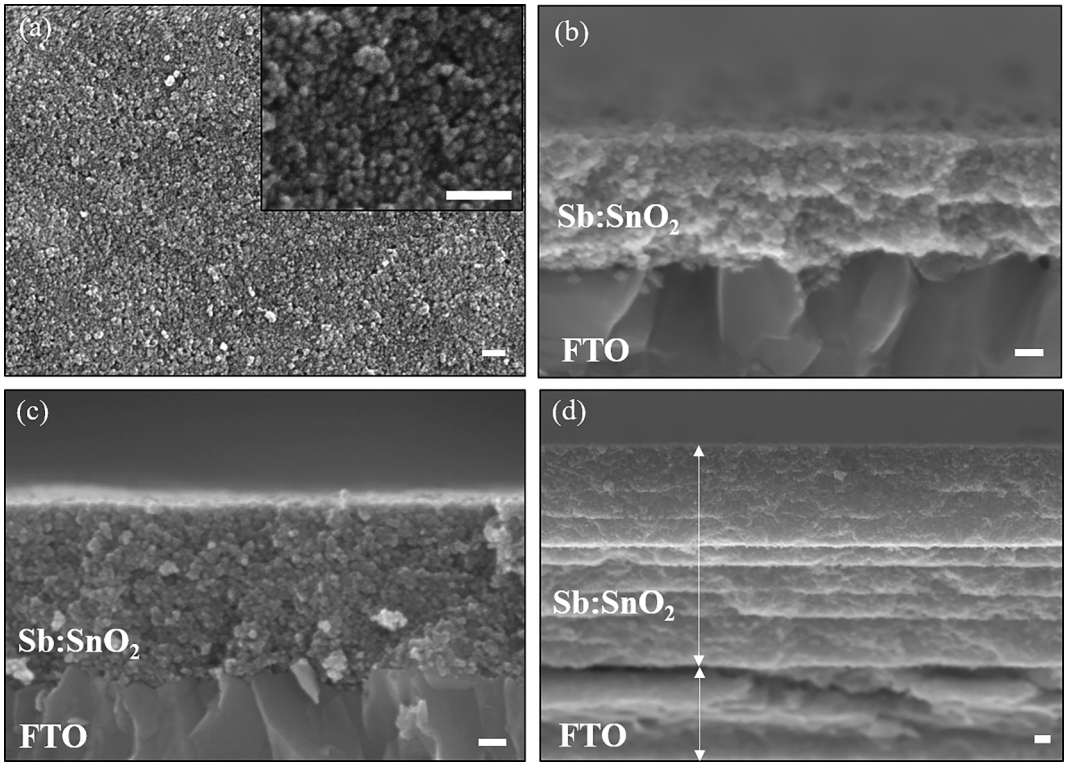

Fig. 2. SEM images of the different Sb:SnO_2 films prepared. (a) Top view of the sample with 5 layers. (b-d) Cross-sectional views of the 2, 5 and 10-layer films, respectively. All scale bars shown are 100 nm width.

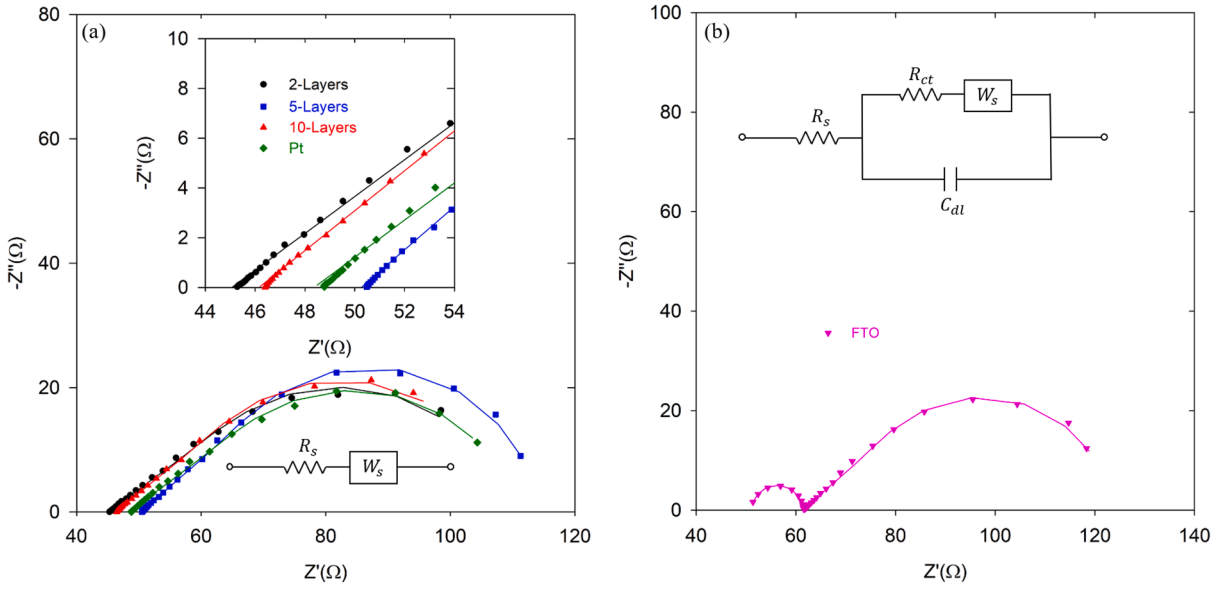

Fig. 3. Impedance results (Nyquist plots) for (a) the cells with the Sb:SnO_2 films and the Pt electrodes and (b) the FTO-only cell. The lines are the fittings performed using the equivalent circuits in the insets.

Table 1
Temperature coefficient (α), series (R_s) and charge-transfer (R_{ct}) resistances, double-layer capacitance (C_{dl}), mass-transfer resistance (R_{mt}), exponent (p) and R_{dc} of the different thermo-electrochemical cells when $\Delta T = 10$ K. Relative errors are shown between brackets. The maximum power output density (P_{max}) and the Carnot-related efficiencies (η_r) are also indicated.

	α (mV/K)	R_s (Ω)	R_{ct} (Ω)	C_{dl} (μF)	R_{mt} (Ω)	p	R_{dc} (Ω)	P_{max} (mW/m^2)	η_r (%)
2 layers	1.20 (0.36 %)	45.1 (0.12 %)	–	–	64.6 (1.00 %)	0.410 (0.66 %)	110	6.55	0.040
5 layers	1.21 (0.89 %)	50.3 (0.10 %)	–	–	64.0 (0.53 %)	0.459 (0.48 %)	114	6.42	0.040
10 layers	1.24 (0.10 %)	46.1 (0.13 %)	–	–	63.0 (1.08 %)	0.428 (0.66 %)	109	6.80	0.042
FTO/ Pt	1.46 (0.19 %)	48.4 (0.17 %)	–	–	62.5 (0.98 %)	0.408 (0.49 %)	111	9.60	0.059
Glass/FTO	1.29 (0.13 %)	51.2 (0.32 %)	10.0 (1.73 %)	0.603 (4.59 %)	62.5 (0.97 %)	0.46 (0.83 %)	124	6.71	0.041

present in the TECs with the ATO and Pt electrodes (Fig. 3a), which indicates a fast charge-transfer kinetics for the ATO TECs, similar to the Pt electrodes, which is a remarkable result, since this is not always the case for many electrode materials [19,24–27]. It should be noticed that the kinetics is not influenced by the electrode surface area, which increases with the ATO film thickness (number of layers), since a lack of a charge-transfer resistance is already observed in Fig. 3a for the thinnest film (2 layers, 320 nm). Related to the good kinetics, we found that Sb:SnO_2 has already been reported to display high faradaic currents on cyclic voltammograms when it was brought into contact with the ferro/ferricyanide electrolyte (same redox reaction) [28].

Fig. 3 and Table 1 also show similar values of R_s in all cases. This is expected, since the main contributions to R_s, the resistance of the substrate (FTO) and the electrolyte resistance, are both the same in all the systems [29]. Concerning the mass transport of the redox species (R_{mt}), all the values are again similar, which is expected since all the cells are formed by the same electrolyte and have the same interelectrode distance.

In order to compare the performance (power output at $\Delta T = 10$ K) of all the systems, the value of the temperature coefficient and the dc resistance R_{dc} was considered. This dc resistance governs the slope of the current–voltage (*I-V*) curve, and comprises the addition of all the resistances extracted from the impedance analysis ($R_{dc} = R_s + R_{ct} + R_{mt}$) [30]. In other words, the impedance spectroscopy analysis can extract all the different contributions behind the value of the slope of the *I-V* curve. Hence, if the values of the open-circuit voltage ($V_{oc} = \alpha\Delta T$) and R_{dc} are known, the maximum power density can be obtained as [$P_{max} = {V_{oc}}^2/(4AR_{dc})$] (see Fig. S2 and the values in Table 1) [30]. As shown in Table 1, the values obtained for α were very close to 1.24 mV/K in all cases, except for FTO/Pt that showed a somewhat larger value (1.46 mV/K). All the values agree with the literature for this electrolyte, which show variations from 1.2 to 1.6 mV/K [6,31].

Analyzing the R_{dc} values, it can be seen from Table 1 that for all the systems, the value is very similar (≈110 Ω), except for the cell with only FTO, which shows a higher value due to the presence of the charge-transfer resistance. It is interesting to note that R_{dc} is basically the same for all the TECs with the ATO layers, and thus the maximum power density. Hence, no increase in P_{max} was obtained due to the increase of the electrode area in contact with the electrolyte, which significantly increases (from 2 to 5 and 10 layers). This occurs since R_{ct} is negligible in all cases and R_{mt} is not affected by the surface area of the electrode, but by the electrolyte channel area. We would like to remark that it is expected that the electrolyte fully permeates the whole ATO electrode, due to its nanostructured and porous nature. In order to support this, we show in Fig. S1 how a solid electrolyte, with even higher viscosity than the ferro/ferricyanide aqueous electrolyte, can permeate an ATO film prepared by us under the same conditions.

The Carnot-related efficiencies of the TECs $\eta_r = \eta[\Delta T/T_H]$, being $\eta =$

$P_{max}/(\kappa\Delta T/d)$, were also estimated, assuming the thermal conductivity of the electrolyte $\kappa = 0.5$ W/(m K). It should be noted that this way of estimating the efficiency, although commonly used, can lead to values somewhat far from reality, since it neglects several heat transfer processes that actually occur (e.g. conduction through the PTFE cell, convection and radiation, etc.) [32]. The η_r value obtained for the FTO/Pt TEC agrees well with the literature [30,31], and it is remarkable that with only 2 layers of ATO, a value in the same order of magnitude can be reached (see Table 1), at a much smaller cost.

4. Conclusions

We have fabricated thermo-electrochemical cells with nanostructured and porous Sb-doped tin oxide films deposited on F:SnO_2 (FTO) glasses as electrodes. Three different thickness of the films were evaluated (320, 550 and 1550 nm). The standard 0.4 M ferro/ferricyanide aqueous electrolyte was used. An impedance spectroscopy analysis under operating conditions revealed that the charge-transfer resistance was negligible for all the different thickness, indicating excellent kinetics, as it is the case for the typically employed expensive Pt electrodes. On the other hand, the temperature coefficients and the series and mass-transport resistances were similar, which led to similar power outputs. Hence, no performance improvements were obtained when the electrode area in contact with the electrolyte was significantly increased. The Carnot-related efficiencies estimated for the Sb:SnO_2 cells were in the same order of magnitude as for Pt electrodes. These results show Sb:SnO_2 as an excellent electrode material for thermo-electrochemical cells, providing similar performance than Pt at a much lower cost.

CRediT authorship contribution statement

Sergio Castro-Ruiz: Writing – original draft, Visualization, Validation, Methodology, Investigation, Formal analysis. **Jorge García-Cañadas:** Writing – review & editing, Visualization, Supervision, Resources, Project administration, Methodology, Funding acquisition, Formal analysis, Conceptualization.

Declaration of competing interest

The authors declare that they have no known competing financial interests or personal relationships that could have appeared to influence the work reported in this paper.

Data availability

The research data is available at Zenodo

Acknowledgements

This project has received funding from the European Union's Horizon 2020 research and innovation programme under grant agreement No 863222 (UncorrelaTEd project). Mauricio Solís and Lourdes Márquez are acknowledged for their technical support.

Appendix A. Supplementary data

Supplementary data to this article can be found online at https://doi.org/10.1016/j.elecom.2024.107683.

References

[1] Q. Hassan, A.M. Abdulateef, S.A. Hafedh, A. Al-samari, J. Abdulateef, A.Z. Sameen, H.M. Salman, A.K. Al-Jiboory, S. Wieteska, M. Jaszczur, Renewable energy-to-green hydrogen: A review of main resources routes, processes and evaluation, Int. J. Hydrogen. Energy 48 (2023) 17383–17408. https://doi.org/10.1016/j.ijhydene.2023.01.175.

[2] M. Luberti, R. Gowans, P. Finn, G. Santori, An estimate of the ultralow waste heat available in the European Union, Energy 238 (2022) 121967. https://doi.org/10.1016/j.energy.2021.121967.

[3] R. Kothari, V.V. Tyagi, A. Pathak, Waste-to-energy: A way from renewable energy sources to sustainable development, Renew. Sustain. Energy. Rev. 14 (2010) 3164–3170. https://doi.org/10.1016/j.rser.2010.05.005.

[4] S. Hur, S. Kim, H.-S. Kim, A. Kumar, C. Kwon, J. Shin, H. Kang, T.H. Sung, J. Ryu, J. M. Baik, H.-C. Song, Low-grade waste heat recovery scenarios: Pyroelectric, thermomagnetic, and thermogalvanic thermal energy harvesting, Nano. Energy 114 (2023) 108596. https://doi.org/10.1016/j.nanoen.2023.108596.

[5] H. Zhou, H. Inoue, M. Ujita, T. Yamada, Advancement of electrochemical thermoelectric conversion with molecular technology, Angew. Chem. Int. Ed. 62 (2023) e202213449. https://doi.org/10.1002/anie.202213449.

[6] J. Duan, B. Yu, L. Huang, B. Hu, M. Xu, G. Feng, J. Zhou, Liquid-state thermocells: Opportunities and challenges for low-grade heat harvesting, Joule 5 (2021) 768–779. https://doi.org/10.1016/j.joule.2021.02.009.

[7] M.A. Buckingham, S. Hammoud, H. Li, C.J. Beale, J.T. Sengel, L. Aldous, A fundamental study of the thermoelectrochemistry of ferricyanide/ferrocyanide: Cation, concentration, ratio, and heterogeneous and homogeneous electrocatalysis effects in thermogalvanic cells, Sustain, Energy. Fuels 4 (2020) 3388–3399, https://doi.org/10.1039/d0se00440e.

[8] W. Li, J. Ma, J. Qiu, S. Wang, Thermocells-enabled low-grade heat harvesting: challenge, progress, and prospects, Mater. Today. Energy 27 (2022) 101032. https://doi.org/10.1016/j.mtener.2022.101032.

[9] L. Zhang, T. Kim, N. Li, T.J. Kang, J. Chen, J.M. Pringle, M. Zhang, A.H. Kazim, S. Fang, C. Haines, D. Al-Masri, B.A. Cola, J.M. Razal, J. Di, S. Beirne, D. R. MacFarlane, A. Gonzalez-Martin, S. Mathew, Y.H. Kim, G. Wallace, R. H. Baughman, High power density electrochemical thermocells for inexpensively harvesting low-grade thermal energy, Adv. Mater. 29 (2017) 1605652–1605659, https://doi.org/10.1002/adma.201605652.

[10] M.S. Romano, N. Li, D. Antiohos, J.M. Razal, A. Nattestad, S. Beirne, S. Fang, Y. Chen, R. Jalili, G.G. Wallace, R. Baughman, J. Chen, Carbon nanotube-reduced graphene oxide composites for thermal energy harvesting applications, Adv. Mater. 25 (2013) 6602–6606, https://doi.org/10.1002/adma.201303295.

[11] R. Hu, B.A. Cola, N. Haram, J.N. Barisci, S. Lee, S. Stoughton, G. Wallace, C. Too, M. Thomas, A. Gestos, M.E. Dela Cruz, J.P. Ferraris, A.A. Zakhidov, R. H. Baughman, Harvesting waste thermal energy using a carbon-nanotube-based thermo-electrochemical cell, Nano. Lett 10 (2010) 838–846, https://doi.org/10.1021/nl903267n.

[12] H. Im, T. Kim, H. Song, J. Choi, J.S. Park, R. Ovalle-Robles, H.D. Yang, K.D. Kihm, R.H. Baughman, H.H. Lee, T.J. Kang, Y.H. Kim, High-efficiency electrochemical thermal energy harvester using carbon nanotube aerogel sheet electrodes, Nat. Commun 7 (2016) 10600, https://doi.org/10.1038/ncomms10600.

[13] W. Li, J. Ma, J. Qiu, S. Wang, Thermocells-enabled low-grade heat harvesting: challenge, progress, and prospects, Mater. Today. Energy 27 (2022) 101032–110150. https://doi.org/10.1016/j.mtener.2022.101032.

[14] J. Chen, Y. Wang, S. Li, H. Chen, X. Qiao, J. Zhao, Y. Ma, H.N. Alshareef, Porous metal current collectors for alkali metal batteries, Adv. Sci. 10 (2023) 2205695. https://doi.org/10.1002/advs.202205695.

[15] Y. Duan, J. Zheng, N. Fu, Y. Fang, T. Liu, Q. Zhang, X. Zhou, Y. Lin, F. Pan, Enhancing the performance of dye-sensitized solar cells: doping SnO 2 photoanodes with Al to simultaneously improve conduction band and electron lifetime, J. Mater. Chem. A 3 (2015) 3066–3073, https://doi.org/10.1039/C4TA05923A.

[16] P. Simon, Y. Gogotsi, Materials for electrochemical capacitors, Nat. Mater 7 (2008) 845–854, https://doi.org/10.1038/nmat2297.

[17] K.A. Adegoke, N.W. Maxakato, Porous metal oxide electrocatalytic nanomaterials for energy conversion: Oxygen defects and selection techniques, Coord. Chem. Rev. 457 (2022) 214389, https://doi.org/10.1016/J.CCR.2021.214389.

[18] D. Artyukhov, N. Kiselev, E. Boychenko, A. Asmolova, D. Zhelenov, I. Artyukhov, I. Burmistrov, N. Gorshkov, High-power-density thermoelectrochemical cell based on Ni/NiO nanostructured microsphere electrodes with alkaline electrolyte, Nanomaterials 13 (2023) 2290–2304.

[19] X. Zhuang, H. Jin, S. Dai, X. Li, W. Guo, Y. Wang, J. Wu, L. Huang, J. Duan, J. Zhou, Self-Assembled asymmetric electrodes for high-efficiency thermogalvanic cells, Adv. Energy. Mater. 13 (2023) 2302011–2302019. https://doi.org/10.1002/aenm.202302011.

[20] S. Castro-Ruiz, L. Márquez-García, M. Solis-De la Fuente, B. Beltrán-Pitarch, A. Mota-Babiloni, F. Vidan, P. Íñigo-Rabinal, G. Guisado-Barrios, J. García-Cañadas, Power factor improvement in a solid-liquid thermoelectric system formed by Sb:SnO2 in contact with a chromium complex solution, Sustain, Energy. Fuels 7 (2023) 4254–4259, https://doi.org/10.1039/d3se00622k.

[21] A.C. Lazanas, M.I. Prodromidis, Electrochemical Impedance Spectroscopy—A Tutorial, ACS. Measurement. Science. Au 3 (2023) 162–193, https://doi.org/10.1021/ACSMEASURESCIAU.2C00070/SUPPL_FILE/TG2C00070_SI_001.ZIP.

[22] A. Lasia, Electrochemical impedance spectroscopy and its applications, Springer New York, 2014. https://doi.org/10.1007/978-1-4614-8933-7.

[23] P. Yang, H. Fan, Electrochemical Impedance Analysis of Thermogalvanic Cells, Chem. Res. Chin. Univ 36 (2020) 420–424, https://doi.org/10.1007/s40242-020-0126-y.

[24] Y. Wang, M. Mukaida, K. Kirihara, L. Lyu, Q. Wei, Poly(3,4-Ethylene Dioxythiophene)/Poly(Styrene Sulfonate) Electrodes in Electrochemical Cells for Harvesting Waste Heat, Energ. Technol. 8 (2020) 1900998. https://doi.org/10.1002/ente.201900998.

[25] K. Wijeratne, U. Ail, R. Brooke, M. Vagin, X. Liu, M. Fahlman, X. Crispin, Bulk electronic transport impacts on electron transfer at conducting polymer

electrode–electrolyte interfaces, Proc. Natl. Acad. Sci. U. S. A 115 (2018) 11899–11904, https://doi.org/10.1073/pnas.1806087115.
[26] K. Wijeratne, M. Vagin, R. Brooke, X. Crispin, Poly(3,4-ethylenedioxythiophene)-tosylate (PEDOT-Tos) electrodes in thermogalvanic cells, J. Mater. Chem. A. Mater 5 (2017) 19619–19625, https://doi.org/10.1039/c7ta04891b.
[27] S.M. Jung, J. Kwon, J. Lee, I.K. Han, K.S. Kim, Y.S. Kim, Y.T. Kim, Cost-efficient nickel-based thermo-electrochemical cells for utilizing low-grade thermal energy, J. Power. Sources 494 (2021) 229705, https://doi.org/10.1016/j.jpowsour.2021.229705.
[28] M.A. Pellitero, Á. Colina, R. Villa, F.J. del Campo, Antimony tin oxide (ATO) screen-printed electrodes and their application to spectroelectrochemistry, Electrochem. Commun 93 (2018) 123–127, https://doi.org/10.1016/j.elecom.2018.06.012.
[29] M. Massetti, F. Jiao, A.J. Ferguson, D. Zhao, K. Wijeratne, A. Würger, J. L. Blackburn, X. Crispin, S. Fabiano, Unconventional Thermoelectric Materials for Energy Harvesting and Sensing Applications, Chem. Rev 121 (2021) 12465–12547, https://doi.org/10.1021/acs.chemrev.1c00218.
[30] S. Castro-Ruiz, J. García-Cañadas, Impedance Spectroscopy Analysis of a Thermo-Electrochemical Cell Under Operating Conditions, in, International Workshop on Impedance Spectroscopy (IWIS) 2022 (2022) 25–27.
[31] T.I. Quickenden, Y. Mua, A Review of Power Generation in Aqueous Thermogalvanic Cells, J. Electrochem. Soc 142 (1995) 3985–3993.
[32] M.A. Trosheva, M.A. Buckingham, L. Aldous, Direct measurement of the genuine efficiency of thermogalvanic heat-to-electricity conversion in thermocells, Chem. Sci. 13 (2022) 4984–4998, https://doi.org/10.1039/d1sc06340e.